J. Earth Syst. Sci. (2022)131 129
https://doi.org/10.1007/s12040-022-01886-1

Upper layer characteristics of the South Eastern Arabian Sea associated with an unusual low saline pool during fag end of southwest monsoon

S Vishnu Narayanan Nampoothiri[1,2,*], Muhammad Shafeeque[1], V S Arun[1,2], B R Smitha[1], Kusum Komal Karati[1], K Rasheed[1], C R Asha Devi[1] and Hashim Manjebrayakath[1]

[1]*Centre for Marine Living Resources and Ecology, Ministry of Earth Sciences, Kochi 682 508, India.*
[2]*School of Marine Sciences, Cochin University of Science and Technology, Kochi 682 016, India.*
**Corresponding author. e-mail: vish4well@gmail.com*

MS received 1 July 2021; revised 28 January 2022; accepted 31 January 2022

Observational evidence on an anomalous low saline pool due to excess rainfall and runoff during September 2020 in the South Eastern Arabian Sea (SEAS) is explained based on *in-situ* and satellite/reanalysis datasets. The study shows the presence of a low saline pool in the coast to offshore section between 10 and 14°N, which is associated with weak winds (3–5 m/s) and surface currents (0.1–0.2 m/s), compared to the long-term average. The pool is observed with strong vertical temperature gradient of 4°C and salinity gradient of 3.5 psu in the upper 20 m column. Cyclonic eddy in the central SEAS influences the distribution of low saline pool which suppress the coastal upwelling in the region. However, active upwelling is observed (surface temperature <26°C) in the southern transects (8–9°N) associated with strong wind (>6 m/s) and surface current (>0.2 m/s) which is also supported with weak rainfall and runoff. The high phytoplankton biomass in the nutrient-rich active upwelling region supports high zooplankton biomass. Contrastingly, the low saline pool region experienced low nitrate and phosphate concentration resulting into less chlorophyll concentration and that might be a plausible reason for the low zooplankton biomass.

Keywords. Salinity pool; southwest monsoon; coastal upwelling; Arabian Sea; biological response.

1. Introduction

South Eastern Arabian Sea (SEAS) undergoes seasonal reversal of monsoon winds, describing seasons as Summer Monsoon (SM, June–September) and Winter Monsoon (WM, November–February) with two interim Spring Inter Monsoon (SIM, March–May) and Fall Inter Monsoon (FIM, October). Two active seasons, SM and WM are associated with strong coastal currents known as West India Coastal Current (WICC) flowing southward during SM and northwards during WM. The former is wind driven by SM winds, carrying Arabian Sea High Saline Water (ASHSW) to the south (Shetye *et al.* 1990) while the latter is driven by pressure gradient (coastal Kelvin wave-induced) carrying low saline Bay of Bengal

Supplementary materials pertaining to this article are available on the *Journal of Earth System Science* website (http://www.ias.ac.in/Journals/Journal_of_Earth_System_Science).
Published online: 28 May 2022

(BoB) waters to the Arabian Sea (AS) towards north during winter (McCreary *et al.* 1993; Prasanna Kumar *et al.* 2004). This seasonally reversing circulation pattern plays an important role in exchanging the watermass between the AS and BoB and in maintaining the salt balance of the region, which is altered by intense evaporation over AS and immense discharge of fresh water received from BoB (Subramanian 1993; Prasad 1997).

In addition to the organized flow pattern during SM and WM, the region is associated with Lakshadweep low/high (LL/LH), respectively. Basic structure of LL is divergent, resulting in sea level low, while that of LH is convergent, resulting in sea level high in the corresponding seasons. The region is also characterized by intense coastal upwelling driven by combined effect of local and remote forcing (Smitha *et al.* 2008; Shah *et al.* 2015, 2019; Vishnu *et al.* 2020; Shafeeque *et al.* 2021a, b). Mesoscale eddies along the coastal shelf also contribute to the seasonal current pattern and upper layer dynamics (Shyni and Hareesh Kumar 2014; Kumar *et al.* 2020; Shafeeque *et al.* 2021a). The overall process makes the region one of the productive zones in the Indian Ocean (Madhupratap *et al.* 2001). Salinity patterns have a major role in defining the extent of vertical mixing and stability, which in turn regulates the regional hydrodynamics. During WM, the SEAS shelf along the Kerala coast is occupied with low saline BoB waters (Prasanna Kumar *et al.* 2004), whereas during the SM, high rainfall occurs along the West Coast of the peninsula (Gadgil 2003). Runoff from the 41 major and minor rivers along the coast modifies the upper layer hydrodynamics, leaving low saline plumes near the coast. Further, excess rainfall and river discharge during southwest monsoon resulted in a low saline pool in the SEAS region (Hareesh Kumar and Mathew 1997; Hareesh Kumar 2014). This rainfall and river discharge result in enhanced stratification during relaxed wind phases and causes variations in the biological production pattern (Shafeeque *et al.* 2019). Stratification results in reduced mixing in the upper layer, and hence vertical pumping of nutrients. The boundary layer between the low-saline surface and high saline subsurface will act as a barrier that limits the mixing, leading to more heat storage in the upper layer (Thadathil *et al.* 2008). Also, this will result in strengthening the prevailing hypoxia (Naqvi *et al.* 2009), which is common on the SEAS shelf.

Arabian Sea is subjected to rapid changes in the rainfall, wind pattern, and thereby upper layer ecosystem processes. The responses of these changes in the upper layer dynamics are yet to be understood. Inclement weather conditions, increased occurrence of cyclones and anomalous rain events are frequent in recent decades. In this context, the present study is an observational report on the hydrodynamics of the SEAS shelf during September 2020, and attempt to explain the biological response to the upper layer hydrodynamics.

2. Data and methods

In-situ observation is carried out along eight transects to understand the hydrography and physical processes during fag end of southwest monsoon (September 2020) along the SEAS (figure 1). A total of 40 hydrographic stations were sampled in the study area along transects off Trivandrum (8°18′N), Kollam (9°N), Kochi (10°N), Ponnani (10°54′N), Kannur (12°N), Mangalore (12°48′N), Karwar (14°30′N) and Goa (15°30′N) transects. The sampling is planned from the coast to offshore at 30, 50, 100, 200, 1000 m isobaths along the eight transects.

2.1 *In-situ data*

In-situ data used for the present study was collected during the cruise onboard Fishery

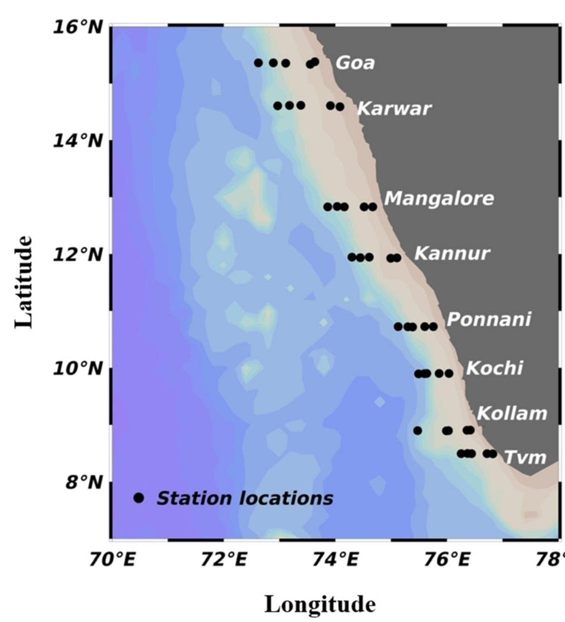

Figure 1. Location map of the study area (South Eastern Arabian Sea) indicating sampling stations (black colour dots).

Oceanography Research vessel (FORV) Sagar Sampada (Cruise no. 399) from 21 September to 10 October 2020 from Trivandrum (8°18′N) to Goa (15°30′N). An additional *in-situ* ship-borne CTD-derived datasets on temperature and salinity onboard Sagar Sampada during September 2003 along the same region were also considered to compare the hydrography and the prevailing processes during the month. Vertical profiles on temperature, salinity, and Sigma-t were measured using CTD. The Sea Bird (SBE 911 Plus) CTD has an accuracy of conductivity ±0.0003 S/m, temperature ±0.001°C, and pressure 0.015%. Water samples were collected using Niskin samplers attached to the CTD Rosette. Salinity measurements are validated against measurements done with a Guildline 8400 Autosal and showed high correlation ($R^2 = 0.847$).

Zooplankton was collected by the vertical hauling of the zooplankton net from the bottom of the mixed layer to the surface water in each sampling location. The mesh size of the net is 200 μm, and the mouth area was 0.25 m^2. The displacement volume method was followed for the estimation of zooplankton biomass, and expressed as ml m^{-3} (Harris *et al.* 2000).

The Brunt–Vaisala frequency, also known as dynamic stability, represented by 'N' in cycl/hr gives a better measure of the stability of oceanic water column, thus a value of >0 cycl/hr indicates stable stratification, 0 cycl/hr neutral stratification and <0 cycl/hr unstable stratification (Gill 1982). To determine the stability of the water column in the SEAS, Brunt–Vaisala frequency was computed as follows:

$$N = \sqrt{-\frac{g}{\rho} \times \frac{d\rho}{dz}}, \qquad (1)$$

where 'g' is the gravitational acceleration (9.8 m/s^2) and 'ρ' is the seawater density (1025 kg/m^3) and '$d\rho/dz$' is the vertical gradient of density (Pond and Pickard 1993). If the water is more stratified, N is higher and if less stratified, N is lower.

2.2 *Satellite and reanalysis data*

Datasets of temperature and geostrophic currents (http://marine.copernicus.eu/faq/cite-cmems-products-cmems-credit/?idpage=169) with a spatial resolution of 0.25°×0.25° were derived from Multi Observation Global Ocean ARMOR3D L4 analysis and multi-year reprocessing (Guinehut *et al.* 2012; Mulet *et al.* 2012).

Weekly salinity product consists of global gap-free Level-4 (L4) analyses of the sea surface salinity (SSS) obtained through a multivariate optimal interpolation algorithm that combines soil moisture ocean salinity (SMOS) satellite images and *in-situ* salinity measurements with satellite SST information (Droghei *et al.* 2018) (http://marine.copernicus.eu/faq/cite-cmems-products-cmems-credit/?idpage=169) were also used. Data are available on a 1/4 degree regular grid and 0.25° × 0.25° spatial resolution and averaged over the observation period.

Daily-averaged wind have been estimated over global oceans from ASCAT retrievals using objective methods which is used to compute wind anomaly during the observation period. The analyses use standard products ASCAT L2b during the period April 2007 through March 2009, and ASCAT L2b 12.5 from April 2009 to 2020 (http://apdrc.soest.hawaii.edu/datadoc/ascat.php). The resulting fields have spatial resolutions of 0.25° (Bentamy and Fillon 2012).

The Global Precipitation Climatology Project (GPCP) monthly rainfall with spatial resolution of 2.5°×2.5° was used to quantify the monthly rainfall anomaly during the observation period. The currently operational procedure is described in Adler *et al.* (2003) and Huffman *et al.* (2009) and has been used to produce the GPCP Version 2.2 Combined Precipitation Data Set, covering the period January 1979 to present (http://apdrc.soest.hawaii.edu/las/v6/constrain?var=12910). The monthly rainfall data with 2.5°×2.5° spatial resolution from CPC Merged Analysis of Precipitation (CMAP) (Xie and Arkin 1997) was also considered and found to agree with the GPCP rainfall datasets.

Climate Forecast System Reanalysis (CFSR) runoff product from the NCEP with a resolution of 0.2° × 0.2° was used to quantify the water runoff over the study region. This product was upgraded to version 2 in March 2011 (Saha *et al.* 2010) and later in 2014. CFSR is the first reanalysis produced from a coupled climate atmosphere–ocean–land surface system with an interactive sea-ice component, which uses a 3D-VAR data assimilation based on the grid-point statistical interpolation scheme (Saha *et al.* 2010). CFSR has been widely used for hydrologic model evaluations and to study the water budget components (Auerbach *et al.*

2016) and was found to outperform all other runoff reanalysis products in the Indian region (Mahto and Mishra 2019).

Daily datasets on biogeochemical parameters derived from numerical model output (NEMO version v3.6_STABLE) with a spatial resolution of 0.25° × 0.25° is used for the present analysis (https://doi.org/10.48670/moi-00015). The parameters chlorophyll, nitrate, phosphate, and silicate for the study region during the observation period were considered to understand the biogeochemical response due to the low saline pool. As this work lacks *in-situ* nutrients and chlorophyll data, we have used the model data to supplement our results from the ship-borne hydrography datasets. It is found that the *in-situ* evidence and derived conclusions are comparable with the model datasets.

3. Results

3.1 *Upper layer characteristics: in-situ evidence*

The SST was found to be in the range of 25–29°C during the observation period with the lowest value (25°C) in the 8–9°N (Trivandrum and Kollam transects) coastal stations. A strong density gradient is observed in the 10–20 m depth level upon analyzing the vertical profiles of temperature and salinity, and hence structured the analysis focussing the same. Isosurface map was drawn at surface, 10 m and 20 m depths that showed a drastic change in the temperature profile (1°C) at each level. Temperature along 10 m isobath ranged between 24 and 29°C, whereas along the 20 m isobaths it ranged between 23 and 29°C (figure 2). The surface layer was relatively warm all along the coast except at 8–9°N, while at 10 m and 20 m, low temperature waters were occupied near the coast in the latitudinal range between 8 and 14°N. The former was observed in pockets, while the latter was continuous along the coast. Surface salinity during the period showed a range of 32–35, whereas at 10 m, it was 34–36, while the horizontal gradient again increased at 20 m to a range of 35–36 (figure 2). The distribution pattern demarcates a low saline pool on the surface up to 10 m, spread over the coast to the oceanic region (150–200 km from the coast), for the 10–14°N section. Mixed layer depth along the SEAS calculated using density criteria (0.2 kg/m^3 rise from the surface) from *in-situ* data ranged between 8 and 12 m. Temperature and salinity figures (figure S1) using satellite reanalysis products were found to agree with observation with low temperature (intense upwelling) along southern regions (8–9°N) and low saline waters in the central SEAS, 10–14°N).

To confirm the anomalous feature in the upper layer hydrography, an additional *in-situ* dataset during September 2003 was also considered and is shown in figure 3. Surface temperature marked 28°C along 8–10°N, whereas it was low (26°C) along 12–14°N where signals of upwelling were dominant. Temperature along 12–14°N was observed to be much lower, recording 24°C and 23°C along 10 m and 20 m isobaths. Salinity was generally high (>34.5) in 2003 compared to 2020, which supports that the low saline pool in September 2020 is anomalous.

3.2 *Latitudinal variation of temperature and salinity*

Temperature and salinity profiles along the coastal (30 m), shelf (200 m), and offshore (1000 m) waters of SEAS were analyzed to understand the upwelling and low saline pool dynamics (figure 4). Temperatures along the coastal region showed the lowest value (24°C) up to 9°N, but increased towards the north (>26°C). Salinity showed a high value (34.5) up to 9°N, where the temperature was low. Low saline pool (<34) is observed in the upper 10 m water column from 10°N to further north with high-temperature values (27°C). In continuation to this, a low saline (34–34.5) patch was observed in the offshore region of Goa. Similar to the coastal sections, upsloping of isotherms (D24 and D26) are also visible in the shelf and offshore waters of the southern transect (figure 4). Also, upsloping of D20 is observed in the central SEAS shelf (50 m) and offshore (70 m) waters. The southward flow of ASHSW with salinity greater than 36 is observed in the shelf and offshore waters north of 14°N. The salinity contours (isolines of 34) along the 14°N are observed between the oceanic low saline patch off Goa and the observed low saline pool, resulting in a regional modification in the upper layer hydrography along the coast, shelf, and offshore regions in the northern part.

3.3 *Forcing mechanisms*

3.3.1 *Wind and current anomaly*

The cross-shore wind speed anomaly showed positive values along the northern part (13–15°N), but

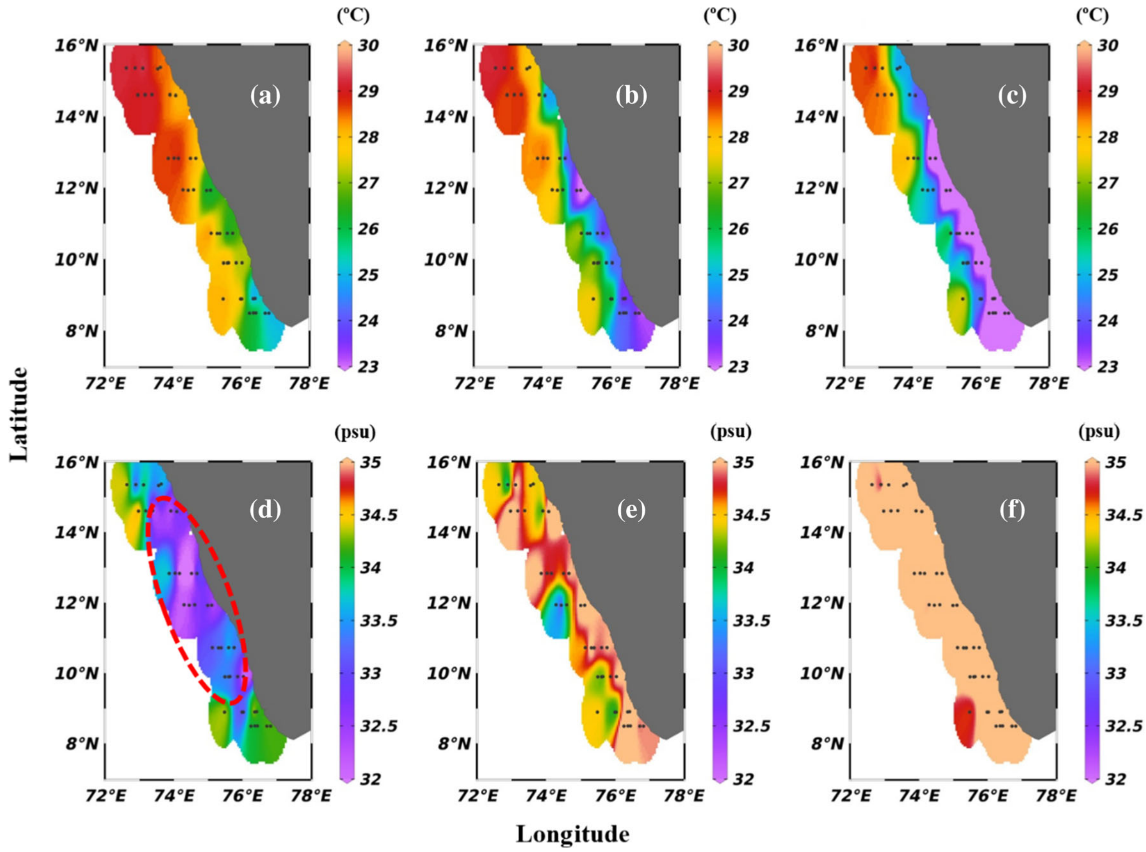

Figure 2. Isosurface maps of temperature (°C). [(**a**) surface, (**b**) 10 m and (**c**) 20 m], and salinity (psu) [(**d**) surface, (**e**) 10 m and (**f**) 20 m] along the SEAS during the observation period (September–October, 2020). Black dots indicate station locations and highlighted area in the salinity map (red colour) indicates low salinity pool.

reduced to negative values along the southern part (8–10°N) indicating strong winds in the north and weak in the south (figure 5). Alongshore wind speed anomalies along the central SEAS showed negative values indicating weak alongshore winds during September 2020, but were observed to be comparatively high along southern (8–9°N) and northern part (14–15°N) (figure 5).

The negative current anomaly was observed along the major part of SEAS (figure 5) indicating weak currents in September 2020 except the northern part (15°N). Total currents during the observation period were irregular and weaker in the coastal region. The total surface currents observed on the surface showed the presence of dominant southward flowing WICC in the offshore regions (figure 5). Currents showed dominant equatorward flow with magnitude ($\sim$0.3 m/s) in the offshore regions, but the coastal stretch was marked with weak currents ($\sim$0.1 m/s) with an irregular pattern. The presence of an anticlockwise circulation (cyclonic eddy) observed along 73–75°E and 7–12°N coincides with the domain of low saline pool. Coastal currents showed strong southward flow in the southern transects off Trivandrum and Kollam (8–9°N) where dominant Ekman transport induced strong coastal upwelling. While north of Kollam, coastal currents were irregular and did not favour coastal upwelling.

3.3.2 *Rainfall and runoff*

Rainfall and runoff anomaly averaged over the observation period along the SEAS shows high positive values (7–15 mm/day and 0.1–0.4 kg/m^2) indicating anomalous feature in the region during September 2020 (figure 6). Offshore regions of central SEAS recorded high rainfall and coastal stretch except 8–9°N shows high amount of runoff to the coast. Maximum value of runoff was observed in the northern part, Karwar to Goa sector (14–16°N). Monthly average rainfall along the SEAS during summer 2020 shows maximum intensity during July (20–30 mm/day), whereas September shows values ranging from 15 to 24 mm/day (figure S2). The anomalous rainfall, especially in the shelf-offshore region and runoff along the coast, weak wind, and currents support

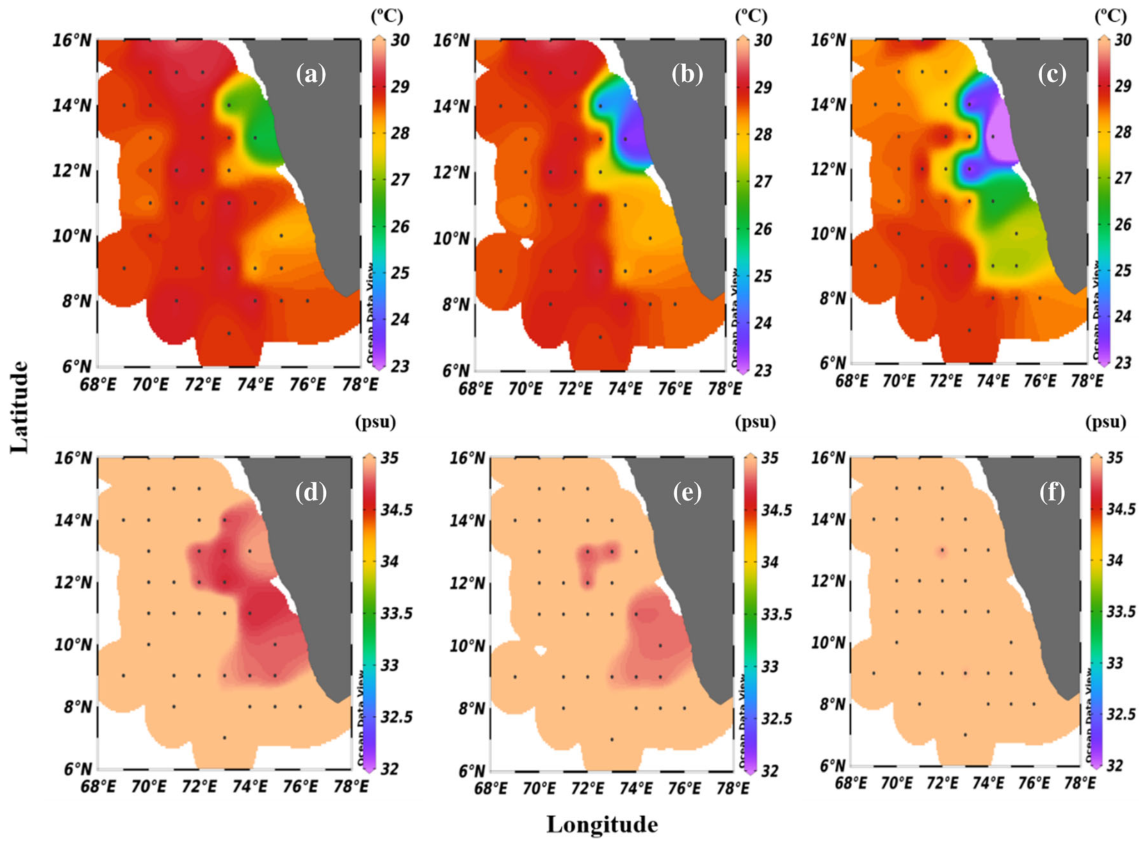

Figure 3. Isosurface maps of temperature (°C) [**(a)** surface, **(b)** 10 m and **(c)** 20 m], and salinity (psu) [**(d)** surface, **(e)** 10 m and **(f)** 20 m] along the SEAS during September 2003. Black dots indicate station locations.

the formation of a low saline pool in the fag end or transition phase of southwest monsoon.

3.4 *Stratification and biological response*

3.4.1 *Stability pattern*

The spatial variation in hydrodynamics associated with the coastal upwelling observed in the southern transects and low saline pool in the central SEAS is addressed based on water column stability using Brunt Vaisala (BV) frequency (figure 7). Stability patterns showed variations in the vertical profiles from south to north. BV profiles along the coast showed weak stratified surface water (0–10 cycl/hr) in the south, but central SEAS was observed as well stratified with a peak value of BV ($\sim$40 cycl/hr) up to 8 m. Surface waters in the northern transects remain neutrally stable (0–10 cycl/hr), but subsurface depths showed well stratified water (30–40 cycl/hr). The upper layer (0–15 m) along the shelf and offshore remains stratified (20–30 cycl/hr) except at northern and southern transects (figure 7). Low saline pool area in the central SEAS showed maximum stability (30–40 cycl/hr) in the upper layers compared to other regions.

3.4.2 *Nutrients, phytoplankton and zooplankton variability*

The surface distribution of nutrients exhibited a prominent spatial variation. Nitrate and phosphate concentration was higher (1.5–2.8 μmol/m^3 and 0.3–0.5 μmol/m^3, respectively) in the active upwelling region in the southern transects, along 8–9°N (figure 8) compared to the northern transects. However, the silicate concentration was higher in the northern low saline pool region along 10–14°N (figure 8) and was maximum (4–6 μmol/m^3) off Goa (15°30′N).

The phytoplankton biomass (chlorophyll) was higher in the active upwelling region than in the low saline pool (figure 8). Zooplankton biomass in the upper mixed layer (ML) also varied widely and ranged between 0.002 and 17.5 ml m^{-3} with an average of 1.5 $\pm$ 3.2 ml m^{-3}. Transect wise, it was relatively higher in the southern part from 8° to 10°N (6.5 $\pm$ 7.7, 2.8 $\pm$ 3.5, and 1.8 $\pm$ 1.9 ml m^{-3} in 8°, 9° and 10°N, respectively). The swarm of

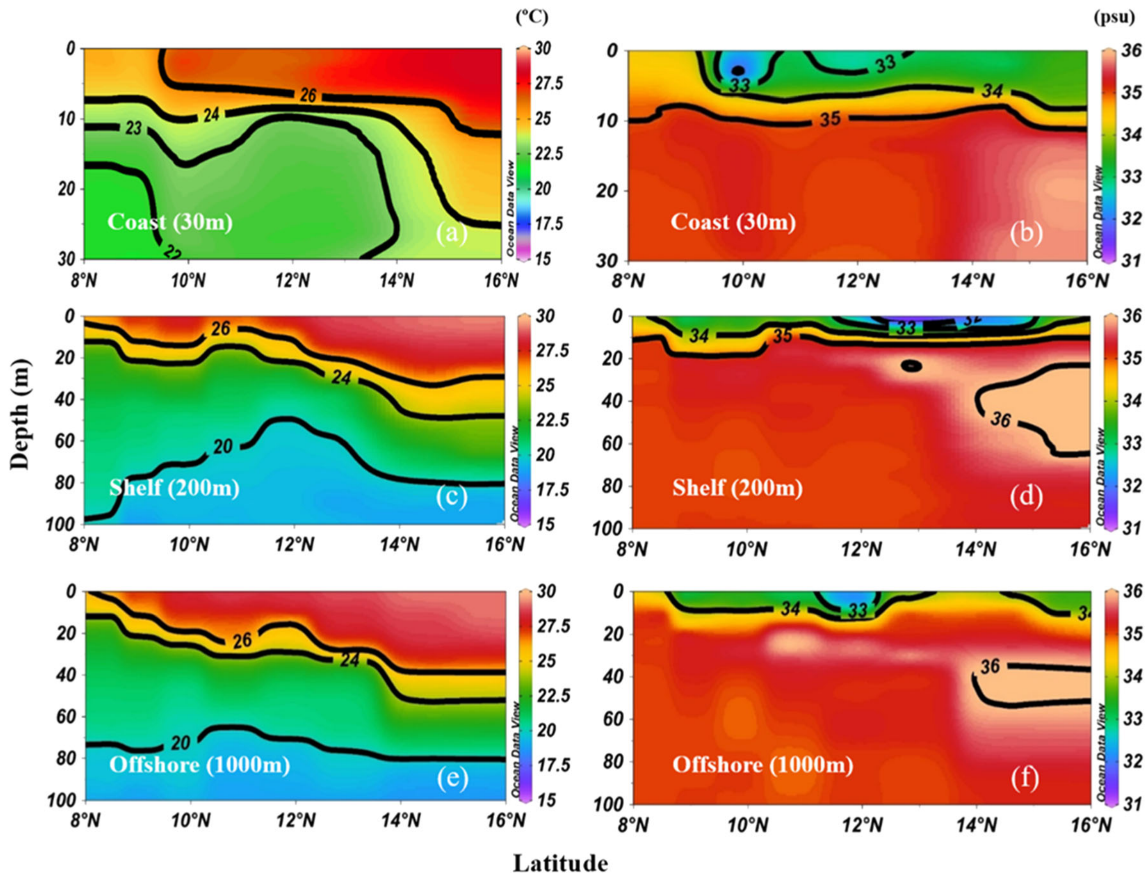

Figure 4. Latitudinal variation of temperature (°C) [**(a)** coastal (30 m), **(b)** shelf (200 m) and **(c)** offshore (1000 m)] and salinity (psu) [**(d)** coastal (30 m), **(e)** shelf (200 m) and **(f)** offshore (1000 m)] along the SEAS.

doliolids had important contributions in the high biomass along 8°N, whereas in the other two transects, the presence of small-sized jellyfish in some of the sampling locations resulted in increased zooplankton biomass. The average biomass was quite less (<0.7 ml m^{-3}) in the northern part when compared to that observed in the southern part (0.3 ± 0.3, 0.04 ± 0.02, and 0.18 ± 0.23 ml m^{-3}, 0.67 ± 0.95, and 0.64 ± 0.57 ml m^{-3}, in 11°, 12°, 13°, 14°, and 15°N, respectively).

4. Discussion

The west coast of India and adjoining SEAS is one of the intense rainfall zones of the Indian summer monsoon. The summer monsoon rainfall in this region is about 1036 km^3 (Behara *et al.* 2019) and the influx of riverine freshwater is maximum along Kochi to Mangalore region (Rao and Sivakumar 2003; Sudheer 2005). Southwest monsoon season in the SEAS is associated with southward dominant surface currents (WICC) (Shetye *et al.* 1990) carrying high saline waters from the north (Shetye *et al.* 1991). The region is also experienced with moderate coastal upwelling during June–September, forced due to the combined action of local southward flowing monsoon winds as well as remote forcing (Smitha *et al.* 2008; Jayaram *et al.* 2012; Smitha *et al.* 2014). The present observation during September records moderate upwelling and the maximum intensity is observed along the southern latitudes (8–9°N) comparable to the results from Vishnu *et al.* (2020) based on the *in-situ* observations.

Generally, coastal waters of SEAS are observed with cold and high saline waters during SM due to coastal upwelling. In the present observation, weak wind speed (<3 m/s) with shallow MLD (10 m) associated with intense rainfall contribute to the suppression of upwelling in the low saline pool region.

Present study records a low saline pool in the upper mixed layer (10 m) that has coast to offshore extension of about 150–200 km covering the central SEAS (figure 2). The presence of this salinity pool extended from Kochi (10°N) to Mangalore (12°42′N), but it was not observed along the region

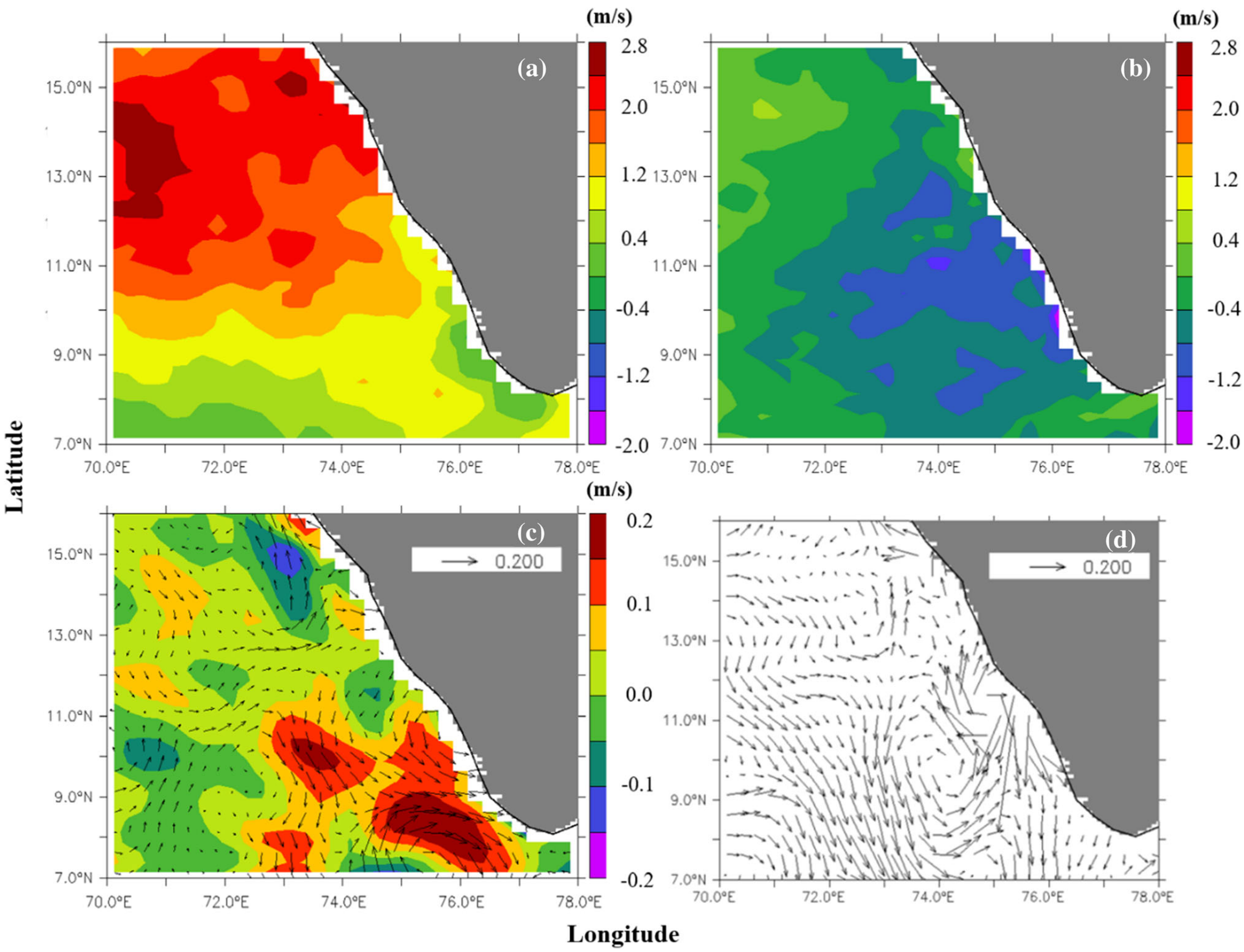

Figure 5. Averaged **(a)** cross-shore windspeed anomaly (u, m/s), **(b)** alongshore windspeed anomaly (v, m/s), **(c)** current speed anomaly (m/s) overlaid with current vector anomaly, and **(d)** surface total currents (m/s) during the observation period along the SEAS.

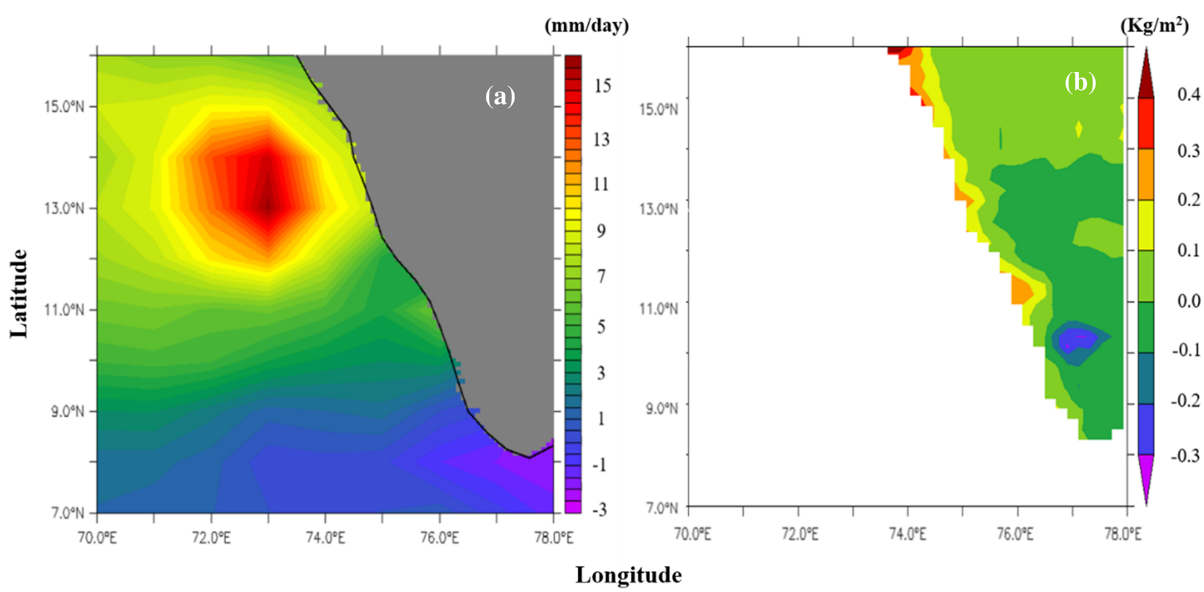

Figure 6. **(a)** Rainfall anomaly (mm/day) and **(b)** runoff anomaly (kg/m^2) averaged over the observation period along the SEAS.

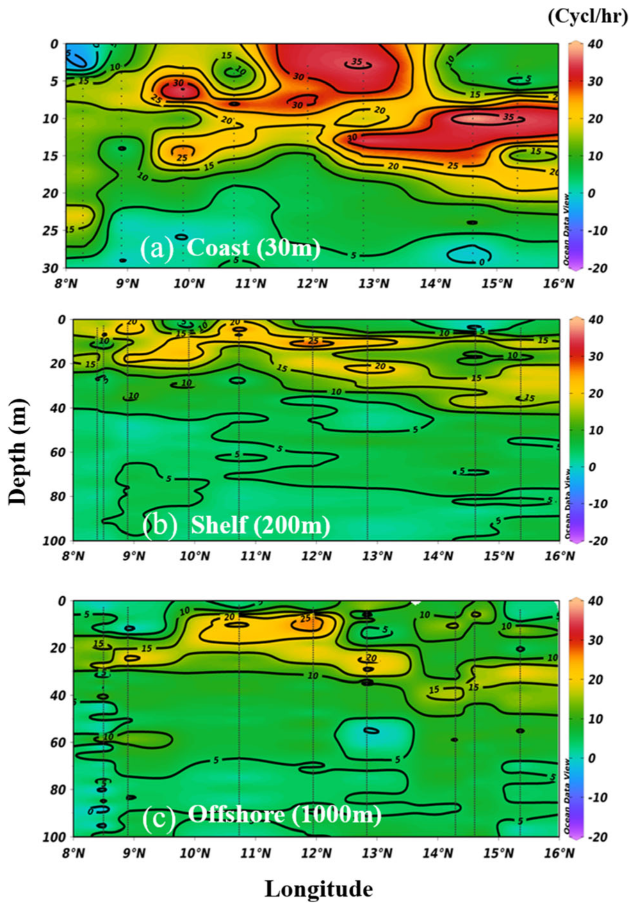

Figure 7. Latitudinal and vertical distribution of *in-situ* derived stability using Brunt–Vaisala frequency (cycl/hr) along the **(a)** coastal (30 m), **(b)** shelf (200 m) and **(c)** offshore (1000 m) waters of SEAS.

south of 9°N (Kollam), where rainfall and freshwater inflow was less; and northern region off Karwar (14°36′N) and Goa (15°18′N) due to presence of high saline waters from the north. In addition, off Goa (15°30′N) was observed with significant coast-offshore variation in salinity, with a low saline pocket (34.5) in the offshore region. Hareesh Kumar and Mathew (1997) also reported low salinity along the west coast of India (15°N) during summer monsoon due to excessive rainfall and river discharge. However, the source, extent and impact of the low saline pool are different from that of the winter monsoon surface waters, which are intruded from BoB, along with poleward WICC.

Observational datasets in the same region during September 2003 (figure 3) were compared for the low saline pool; however, the region was recorded with high saline upwelled waters, evincing weak stratification in the region. Further, the anomaly derived from the climatology and September 2020 observations on the wind, surface currents, rainfall, and river runoff shows that the low salinity pool is an unusual phenomenon in the region (figures 5 and 6). Hareesh Kumar (2014) discussed the low saline pool (<34.5) up to 10 m, during August–September in the southern part of SEAS (up to 10°30′N); however, they attribute the same to the freshwater from the equator and near the coastal region.

The anomalous September rainfall and runoff in 2020, might have increased the freshwater on the surface, resulting in a strong vertical gradient (3.5 in 20 m) in salinity in the upper 20 m (figure 2). Peak rainfall observed in the oceanic region results in the development and trapping of the low saline pool, which was supported by enormous runoff along the coastal stretch. North of the pool region, the strong cross-shore winds, southward flowing WICC carrying ASHSW and resultant mixing suppresses coastal upwelling (Smitha *et al.* 2008; Shah *et al.* 2019) which leads to warmer SST, which is well evident in figure 2. This demarcates the mechanism for suppressing upwelling in the region. Whereas, the alongshore wind speed was less in the pool region and north of pool region compared to southern upwelling zone. The weak coastal currents (<0.1 m/s) and cyclonic eddy, as observed in figure 5, also restricted the active flow towards the south, thus trapping the low-saline water in the central SEAS.

Below 10 m, temperature and salinity showed sharp gradients with salinity increasing to around 35. *In-situ* observations during the active upwelling in the SEAS record SST in the range of 22.8°–28°C, as observed in the previous studies onboard *FORV Sagar Sampada* (Sree Renjima and Sanjeevan 2018). Considering these variations, the reference isotherm for tracking upwelling is kept as D23. D23 can be used as a good index for thermocline undulations, as reported by Fernandez *et al.* (2019). The 23°C isotherm marks the presence of upwelling all along the coast at 10 m, in a uniform pattern. The observations indicate that the surfacing of upwelled waters is restricted at south (up to 9°N), while northwards, in the central SEAS the process was suppressed to sub-surface because of the presence of low saline pool, and the prevailing weak wind and surface current. The extent of the low saline pool was controlled by cyclonic eddy spreading the water in a large spatial domain in the east–west, however, restricting its southward flow where intense alongshore Ekman transport (–1030 kg/m/s) and active upwelling dominates (Shah

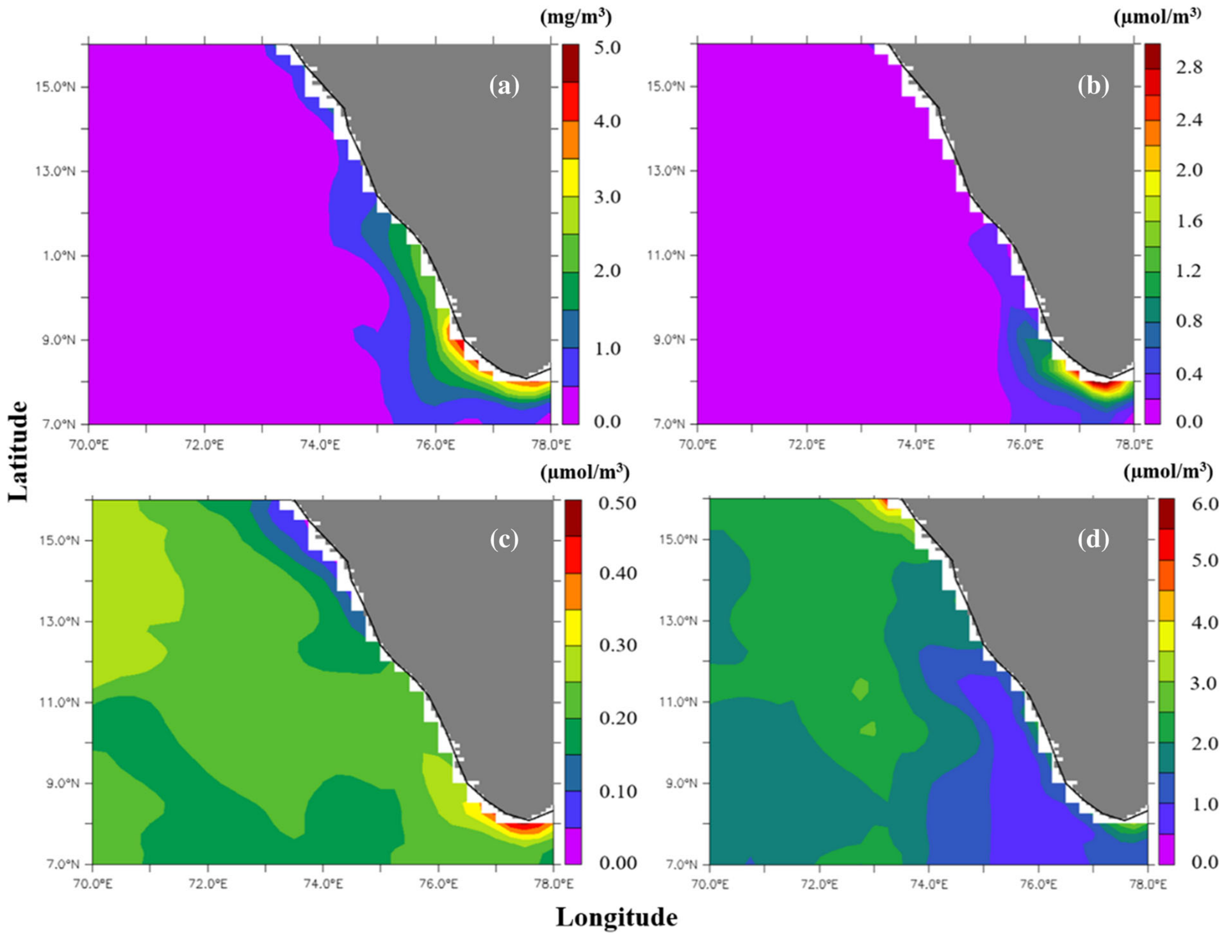

Figure 8. **(a)** Chlorophyll (mg/m^3), **(b)** Nitrate (µmol/m^3), **(c)** Phosphate (µmol/m^3) and **(d)** Silicate (µmol/m^3) averaged over the observation period along the SEAS.

et al. 2015). The spatial extension of the observed cyclonic eddy centered at 10°N, 74°30′E was around 450 km (meridional) and 250 km (zonal), as observed in figure 5. This was identified as a recurring eddy in the SEAS region by Shyni and Hareesh Kumar (2014) and Shafeeque *et al.* (2021a), which is mainly forced by wind stress curl and baroclinic instability due to remote forcing (Shankar and Shetye 1997; Amol 2018; Thushara and Vinayachandran 2020). Less impact in biology is perhaps due to the weak intensity of the observed cyclonic eddy. This low saline pool is observed even beyond shelf up to 1000 depth zone, which again is anomalous from that recorded by Hareesh Kumar (2014), with an increasing salinity towards offshore due to mixing with the strong southward WICC.

The region north to Karwar (14°30′N) was observed with significant spatial variation in salinity (figure 2). A low saline pocket (34.5) was observed off Goa, while the shelf was high saline compared to the near-coastal and the low saline pocket offshore. SEAS, in general, is characterized by coastal upwelling during the observation period; however, southward flow of ASHSW is found to influence the regional salinity pattern with a coast-offshore variability, especially off Goa. This results in spatial variability in the salinity distribution off Goa, leaving a low saline patch in the upper layer and ASHSW in the subsurface offshore region (figure 2). The isolines of salinity (34) along the 14°N are observed between this oceanic low saline patch off Goa and the low saline pool, resulting in a regional modification in the upper layer hydrography.

Vertical stability patterns also showed high stable surface waters in the low saline pool regions (figure 7). Stability maximum was observed at 10 m depth due to the density gradients caused due to low saline pool. Regions of active upwelling were observed to be less stable compared to low saline pool regions. Variability in the atmospheric forcing, hydrodynamics, or the mixed layer characteristics results in changes in the biological characteristics of the ecosystem as well. In a similar study, the anomalous rainfall, runoff, and associated stratification during 2017 were found to be influenced negatively on the strength of upwelling and the landing of Indian oil Sardine fishery (Narvekar *et al.* 2021). The spatial variability in the nutrient distribution might have helped in the distribution of observed chlorophyll concentration (figure 8). The higher concentration of nitrate and phosphate in the active upwelling region in the southern transects compared to the northern low saline pool region is expected as the influence of upwelling on the enrichment of nutrients in this region is well known (Habeebrehman *et al.* 2008). However, the silicate concentration was higher in the low saline pool region, more along the coast, associated with the freshwater discharge (figure 8). The observed high phytoplankton biomass in the nitrate and phosphate-rich upwelling region supported the role of these nutrients on the regional primary production. In association with the higher phytoplankton concentration, the high zooplankton biomass in the southern part indicated the role of phytoplankton in supporting the secondary producers. Although taxon level enumeration of zooplankton community was not carried out during the present study, different zooplankton taxa have been found to have a preference for a particular salinity range in Indian water (figure 10 in Karati *et al.* 2018). Hence, in the low saline pool region, along with low phytoplankton biomass, the unanticipated presence of the low saline upper water might have acted as an unfavorable environment for the zooplankton community resulting in the low biomass.

5. Conclusions

The present study explains the variability in the SEAS hydrodynamics in response to varying ocean-atmospheric forcings (wind, current, rainfall, and runoff) and its impact on the regional ecosystem. September 2020 records excess rainfall and runoff, and *in-situ* ship-based observations during the period in the SEAS, shows the presence of a low saline pool, an unusual distribution pattern of salinity in the region. This low saline pool is well associated with the maximum rainfall pocket in offshore and enormous runoff along the coast, and it is put forward that the weak winds and currents maintain the region as quiescent and stratified. This unusual occurrence is found to suppress the coastal upwelling in the 9–13°N sector, and its impact is indicative of biological production as well. Southern section was supported by strong biological activity due to upwelling resulting in high chlorophyll and zooplankton biomass, while the low saline pool area was stratified and less productive. The study thus put forward that any attempt to explain the ecosystem processes and interactions to be comprehensive, and variability in any of the components explaining the physical drivers to marine life is of concern. Any efforts to ecosystem modelling need to consider these variabilities, especially with rainfall and runoff both in space and time.

Acknowledgements

Authors are grateful to the Secretary, Ministry of Earth Sciences, India and the Director, CMLRE for their encouragement and support. The authors are also grateful to the Vessel Management Cell and all the fellow participants and crew members onboard *FORV Sagar Sampada* (Cr-399) for their support in data collection. The authors wish to acknowledge the use of satellite and reanalysis datasets obtained from https://marine.copernicus.eu, https://cds.climate.copernicus.eu and http://apdrc.soest.hawaii.edu. This is CMLRE contribution no. 149.

Author statement

VNNS: Data collection, planned, analysed and wrote the manuscript. MS and KKK: Data collection, analysis and writing. AVS: Analysis and plotting. SBR and RK: Conceptualization and writing. ACR and HM: Overall supervision and scrutiny of draft manuscript.

References

Adler R F, Huffman G J, Chang A, Ferraro R, Xie P, Janowiak J, Rudolf B, Schneider U, Curtis S, Bolvin D, Gruber A, Susskind J, Arkin P and Nelkin E 2003 The version 2 Global Precipitation Climatology Project (GPCP) monthly precipitation analysis (1979–present); *J. Hydrometeor.* **4(6)** 1147–1167.

Amol P 2018 Impact of Rossby waves on chlorophyll variability in the southeastern Arabian Sea; *Rem. Sens. Lett.* **9(12)** 1214–1223.

Auerbach D A, Easton Z M, Walter M T, Flecker A S and Fuka D R 2016 Evaluating weather observations and the Climate Forecast System Reanalysis as inputs for hydrologic modelling in the tropics; *Hydrol. Process.* **30(19)** 3466–3477.

Behara A, Vinayachandran P N and Shankar D 2019 Influence of rainfall over eastern Arabian Sea on its salinity; *J. Geophy. Res.* **124(7)** 5003-5020.

Bentamy A and Fillon D C 2012 Gridded surface wind fields from Metop/ASCAT measurements; *Int. J. Rem. Sens.* **33(6)** 1729–1754.

Droghei R, Buongiorno Nardelli B and Santoleri R 2018 A new global sea surface salinity and density dataset from multivariate observations (1993–2016); *Front. Mar. Sci.* **5** 84.

Fernandez D R, Rao A R and Niji T Y 2019 Onset and evolution of upwelling along the west coast of India; *Def. Sci. J.* **69(2)** 120–126.

Gadgil S 2003 The Indian monsoon and its variability; *Ann. Rev. Eart. Plan. Sci.* **31(1)** 429–467.

Gill A E 1982 *Atmosphere–ocean dynamics*; Academic Press, San Diego, California, 662p.

Guinehut S, Dhomps A L, Larnicol G and Le Traon P Y 2012 High resolution 3D temperature and salinity fields derived from *in situ* and satellite observations; *Ocean Sci.* **8(5)** 845–857.

Habeebrehman H, Prabhakaran M P, Jacob J, Sabu P, Jayalakshmi K J, Achuthankutty C T and Revichandran C 2008 Variability in biological responses influenced by upwelling events in the Eastern Arabian Sea; *J. Mar. Syst.* **74(1–2)** 545–560.

Hareesh Kumar P V 2014 Salinity variation in the southeastern Arabian Sea: A revisit; *Ind. J. Geo-Mar. Sci.* **43(09)** 1650–1658.

Hareesh Kumar P V and Mathew B 1997 Salinity distribution in the Arabian Sea; *Ind. J. Geo-Mar. Sci.* **26(3)** 271–277.

Harris R, Wiebe P, Lenz J, Skjoldal H R and Huntley M (eds) 2000 ICES zooplankton methodology manual; Elsevier, Academic Press, London, 684p.

Huffman G J, Adler R F, Bolvin D T and Gu G 2009 Improving the global precipitation record: GPCP Version 2.1; *Geophys. Res. Lett.* **36(17)** L17808.

Jayaram C, Udaya B T, Ajith J K and Balchand A N 2012 Application of satellite products to study upwelling, chlorophyll and mixed layer depth of southeastern Arabian Sea; *The Int. J. Ocean Clim. Syst.* **3(2)** 97–108.

Karati K K, Vineetha G, Raveendran T V, Muraleedharan K R, Habeebrehman H, Philson K P and Achuthankutty C T 2018 River plume fronts and their implications for the biological production of the Bay of Bengal, Indian Ocean; *Mar. Ecol. Prog. Ser.* **597** 79–98.

Kumar K V, Rasheed K, Smitha B R, Nampoothiri S V N and Sudhakar M 2020 Description on variability of shelf-edge hydrography and current structure of the South Eastern Arabian Sea during summer and winter monsoons*; Environ. Monit. Assess.* **192(11)** 1–22.

Madhupratap M, Nair K N V, Gopalakrishnan T C, Haridas P, Nair K K C, Venugopal P and Gauns M 2001 Arabian Sea oceanography and fisheries of the west coast of India; *Curr. Sci.* **81(4)** 355–361.

Mahto S S and Mishra V 2019 Does ERA-5 outperform other reanalysis products for hydrologic applications in India?; *J. Geophys. Res.* **124(16)** 9423–9441.

McCreary Jr J P, Kundu P K and Molinari R L 1993 A numerical investigation of dynamics, thermodynamics and mixed-layer processes in the Indian Ocean; *Progr. Ocean.* **31(3)** 181–244.

Mulet S, Rio M H, Mignot A, Guinehut S and Morrow R 2012 A new estimate of the global 3D geostrophic ocean circulation based on satellite data and *in-situ* measurements; *Deep Sea Res.* **77** 70–81.

Naqvi S W A, Naik H, Jayakumar A, Pratihary A K, Narvenkar G, Kurian S and Narvekar P V 2009 Seasonal anoxia over the western Indian continental shelf; In: *Indian Ocean biogeochemical processes and ecological variability* (eds) Wiggert J D, Hood R R, Naqvi S W A, Brink K H, Smith S L, American Geophysical Union, Washington DC, pp. 333–345.

Narvekar J, Chowdhury R R, Gaonkar D, Kumar P D and Kumar S P 2021 Observational evidence of stratification control of upwelling and pelagic fishery in the eastern Arabian Sea; *Sci. Rep.* **11(1)** 1–13.

Pond S and Pickard G L 1993 *Introductory dynamic oceanography*; Pergamon Press, New York, 240p.

Prasad T G 1997 Annual and seasonal mean buoyancy fluxes for the tropical Indian Ocean; *Curr. Sci.* **73(8)** 667–674.

Prasanna Kumar S, Narvekar J, Kumar A, Shaji C, Anand P, Sabu P and Nair K K C 2004 Intrusion of the Bay of Bengal water into the Arabian Sea during winter monsoon and associated chemical and biological response; *Geophys. Res. Lett.* **31(15)** L15304.

Rao R R and Sivakumar R 2003 Seasonal variability of sea surface salinity and salt budget of the mixed layer of the north Indian Ocean; *J. Geophys. Res.* **108(C1)** 9–1.

Saha S, Moorthi S, Pan H L, Wu X, Wang J, Nadiga S, *et al.* 2010 The NCEP Climate Forecast System Reanalysis; *Bull. Am. Meteor. Soc.* **91(8)** 1015–1058.

Shafeeque M, Balchand A N, Shah P, George G, Smitha B R, Varghese E, Ajith J K, Sathyendranath S and Platt T 2021a Spatio-temporal variability of Chlorophyll-*a* in response to coastal upwelling and mesoscale eddies in the southeastern Arabian Sea; *Int. J. Rem. Sens.* **42(13)** 4836–4863.

Shafeeque M, George G, Akash S, Smitha B R, Shah P and Balchand A N 2021b Interannual variability of Chlorophyll-*a* and impact of extreme climatic events in the southeastern Arabian Sea; *Reg. Stud. Mar. Sci.* **48** 101986.

Shafeeque M, Shah P, Platt T, Sathyendranath S, Menon N N, Balchand A N and George G 2019 Effect of precipitation on Chlorophyll-*a* in an upwelling-dominated region along the west coast of India; *J. Coast. Res.* **86(sp1)** 218–224.

Shah P, Sajeev R and Gopika N 2015 Study of upwelling along the west coast of India – A climatological approach; *J. Coast. Res.* **31(5)** 1151–1158.

Shah P, Sajeev R, Thara K J, George G, Shafeeque M, Akash S and Platt T 2019 A holistic approach to upwelling and downwelling along the south-west coast of India; *Mar. Geod.* **42(1)** 64–84.

Shankar D and Shetye S R 1997 On the dynamics of the Lakshadweep high and low in the southeastern Arabian Sea; *J. Geophys. Res.* **102(C6)** 12,551–12,562.

Shetye S R, Gouveia A D, Shenoi, S S C, Sundar D, Michael G S, Almeida A M and Santanam K 1990 Hydrography and circulation off the west coast of India during the southwest monsoon 1987; *J. Mar. Res.* **48(2)** 359–378.

Shetye S R, Gouveia A D, Shenoi S S C, Michael G S, Sundar D, Almedia A M and Santanam K 1991 The coastal current off western India during the northeast monsoon; *Deep Sea Res.* **38** 1517–1529.

Shyni T N and Hareesh Kumar P V 2014 The influence of mesoscale eddies on the current field and thermal structure of the southeastern Arabian Sea; *Int. J. Rem. Sens.* **35(14)** 5479–5496.

Smitha A, Joseph K A, Jayaram C and Balchand A N 2014 Upwelling in the southeastern Arabian Sea as evidenced by Ekman mass transport using wind observations from OCEANSAT–II Scatterometer; *Ind. J. Geo-Mar. Sci.* **43(01)** 111–116.

Smitha B R, Sanjeevan V N, Vimalkumar K G and Revichandran C 2008 On the upwelling off the southern tip and along the west coast of India; *J. Coast. Res.* **24** 95–102.

Sree Renjima G and Sanjeevan V N 2018 Studies on eggs and larvae of Oil Sardine, Indian Mackerel and Anchovy in the South Eastern Arabian Sea Upwelling System (PhD Thesis, Cochin University of Science and Technology).

Subramanian V 1993 Sediment load of Indian rivers; *Curr. Sci.* **64(11/12)** 928–930.

Thadathil P, Thoppil P, Rao R R, Muraleedharan P M, Somayajulu Y K, Gopalakrishna V V and Revichandran C 2008 Seasonal variability of the observed barrier layer in the Arabian Sea; *J. Phys. Ocean.* **38(3)** 624–638.

Thushara V and Vinayachandran P N 2020 Unprecedented surface chlorophyll blooms in the southeastern Arabian Sea during an extreme negative Indian Ocean Dipole; *Geophy. Res. Lett.* **47** 1–11.

Vishnu N N S, Sachin T S and Rasheed K 2020 Dynamics and forcing mechanisms of upwelling along the south eastern Arabian sea during southwest monsoon; *Reg. Stud. Mar. Sci.* **40** 101519.

Xie P and Arkin P A 1997 Global precipitation: A 17-year monthly analysis based on gauge observations, satellite estimates, and numerical model outputs; *Bull. Am. Meteor. Soc.* **78** 2539–2558.

Corresponding editor: C Gnanaseelan